JACS
JOURNAL OF THE AMERICAN CHEMICAL SOCIETY

Article

pubs.acs.org/JACS

# Rational Design of DNA Motors: Fuel Optimization through Single-Molecule Fluorescence

Toma E. Tomov, Roman Tsukanov, Miran Liber, Rula Masoud, Noa Plavner, and Eyal Nir*

Department of Chemistry and the Ilse Katz Institute for Nanoscale Science and Technology, Ben-Gurion University of the Negev, Beer Sheva, 84105, Israel

Supporting Information

**ABSTRACT:** While numerous DNA-based molecular machines have been developed in recent years, high operational yield and speed remain a major challenge. To understand the reasons for the limited performance, and to find rational solutions, we applied single-molecule fluorescence techniques and conducted a detailed study of the reactions involved in the operation of a model system comprised of a bipedal DNA walker that strides on a DNA origami track powered by interactions with fuel and antifuel strands. Analysis of the kinetic profiles of the leg-lifting reactions indicates a pseudo-first-order antifuel binding mechanism leading to a rapid and complete leg-lifting, indicating that the fuel-removal reaction is not responsible for the 1% operational yield observed after six steps. Analysis of the leg-placing reactions showed that although increased concentrations of fuel increase the reaction rate, they decrease the yield by consecutively binding the motor and leading to an undesirable trapped state. Recognizing this, we designed asymmetrical hairpin-fuels that by regulating the reaction hierarchy avoid consecutive binding. Motors operating with the improved fuels show 74% yield after 12 consecutive reactions, a dramatic increase over the 1% observed for motors operating with nonhairpin fuels. This work demonstrates that studying the mechanisms of the reactions involved in the operation of DNA-based molecular machines using single-molecule fluorescence can facilitate rationally designed improvements that increase yield and speed and promote the applicability of DNA-based machines.

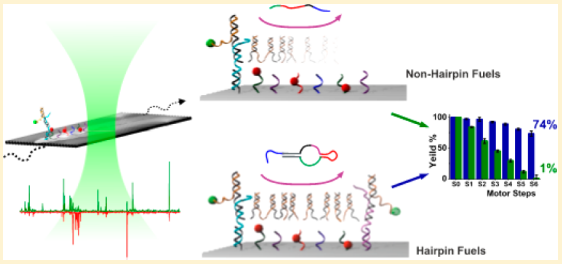


## INTRODUCTION

Natural molecular machines comprised of proteins and RNA display impressive yields and speeds. For example, a bipedal Kinisin motor can walk hundreds of steps at a rate of several steps per second without dissociating from the microtubule track.[1] For fast and efficient *artificial* molecular machines, DNA molecules have several uniquely advantageous properties.[2−6] Structurally, carefully designed DNA strands can be assembled into two-[7−9] and three-dimensional[10−12] DNA-origami structures that adapt unique and predictable conformations[13−17] while providing the structural stability required for the rational design[18] and development of well-functioning machines. Device conformations can be controllably altered by hybridizing specific strands called fuels.[19] These can be connected to a device by a straightforward hybridization reaction. Conversely, they can be disconnected and removed by hybridizing complementary strands, i.e., antifuels,[19] in a reaction called toehold-mediated strand displacement.[20−22] The rates of elementary strand hybridization and toehold-mediated strand displacement (measured not in the context of complex devices) are on the order of from $10^5$ to $10^6$ $M^{-1}$ $s^{-1}$ and the reaction yields approach 100%.[22−25] To illustrate, with these properties, reactions initiated at 1 $\mu$M concentration should reach 99% yield within from 1000 to 100 s, respectively.

Numerous and diverse dynamic devices[19,26−33] and motors[34−37] operating on the basis of these reactions have been demonstrated. The operational yields (defined as the fraction of devices that operate as intended) and speeds of these devices, however, are generally lower than those of elementary hybridization and strand-displacement reactions and of natural molecular machines, hindering the progress of DNA-based nanotechnology.

We now report a detailed single-molecule florescence investigation of an origami-based nonautonomous motor. Using this technique, we identified underlying phenomena responsible for limited rates and yields, and this understanding led directly to a rational solution. The motor is made of a bipedal walker that strides on a robust origami-based track by interaction with sequentially introduced fuel and antifuel strands. We monitored the walker progress as it was striding on the track and found that when the motor was fed with nonhairpin fuels, the yield was low. To understand the reason for the low operational yield, we investigated the mechanisms of the fuel-removal and fuel-addition reactions at a single-molecule level. The kinetic profiles indicated that consecutive binding of two fuels to a single motor was the reason for the low operational yield. In response, we introduced fuels with hairpin structure that, by regulating the reaction hierarchy, prevented consecutive binding. Motors fed with the improved

**Received:** May 14, 2013
**Published:** July 23, 2013

   dx.doi.org/10.1021/ja4048416 | J. Am. Chem. Soc. 2013, 135, 11935−11941

hairpin-fuels operated with dramatically higher yields and with rates approaching those of elementary DNA-strand reactions.

## RESULTS AND DISCUSSION

**Motor Design.** Our motor consists of an origami-based track, a bipedal walker, fuel strands that connect the walker to the track, and antifuel strands that remove the fuels (Figure 1A,C), and it is based on a motor introduced before.[35] In the original motor, the track was made of four footholds that branched out of a one-dimensional helix bundle. Our motor consists of seven footholds (T0–6; see Supporting Information for sequences, S1) that branch out of a two-dimensional rectangle origami,[7] providing stability and enabling longer tracks. The walker is made of two partially hybridized strands, called legs (L1–2). Fuels that contain hairpins are called hairpin-fuels (HF0–4) and classical fuel strands that lack secondary structures are called fuels (F0–4). Each of the five fuels or hairpin-fuels is designed to join one of the two legs to one (or two) of the seven footholds (the T1 sequence was identical to that of T5 and T2 to that of T6). Fuels or hairpin-fuels can be removed from the motor by a strand-displacement reaction, initiated by the introduction of the corresponding antifuel or anti-hairpin-fuel strand (AF0–6 or AHF0–6, respectively). Introduction of the proper sequence of fuels and antifuels, therefore, causes the walker to stride on the track.

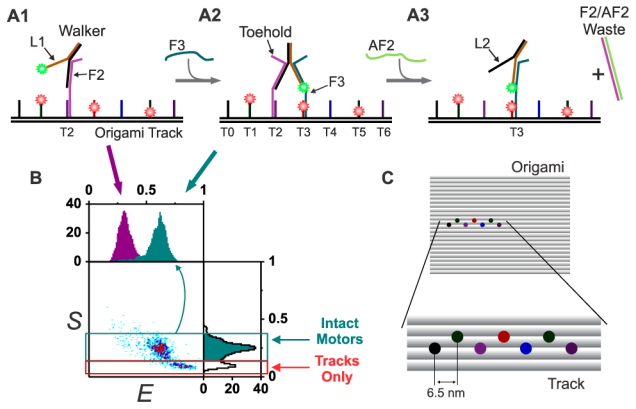


**Figure 1.** Principles of the motor operation and the sm-FRET/ALEX technique. (A1) Fuel F2 connects leg L2 to foothold T2. L1, labeled with a donor fluorophore is lifted and the donor–acceptor(s) distance is large (purple *E*-histogram at (B)). (A2) F3 is added to the solution, joins L1 with T3, and the donor–acceptor distance is shortened (green *E*-histogram). (A3) Antifuel AF2 is added to the solution, binds the toehold of F2, and removes F2 from the motor. The *E* value decreases and a duplex waste is formed. (B) Two dimensional *E*/*S*-histogram and *E*- and *S*-histograms of the motor presented at A2 and an *E*-histogram of the motor presented at A1. Intact motors that consist of one donor and three acceptors yield *S* values centered around 0.25 (inside the dark green rectangle). Origami tracks that have lost the walker consist only of three acceptors yield *S* values centered around 0.1 (inside the red rectangle). The *E*-histograms are constructed only from the population with the correct fluorophores stoichiometry (green rectangle). (C) Top view of the origami track.

**Single-Molecule Measurement.** The motor structure, kinetics, and integrity were measured using single-molecule Förster resonance energy transfer and alternating laser excitation techniques (sm-FRET/ALEX;[38−42] see Supporting Information, S2). The motor was labeled at positions that enabled determining the state and the integrity of the motor. L1 was labeled with a donor fluorophore, and T1, T3, and T5 were each labeled with an acceptor fluorophore at a decreased distance from the origami. With this arrangement, the FRET efficiency (*E*) values indicated to which of the labeled foothold L1 was connected or whether it was lifted (Figure 1B). The fluorophores stoichiometry ratio (*S*) values indicated the presence/absence of the walker and the track. This enables determining the fraction of motors that remained intact and, by rejecting events (molecular species transient through the confocal spot, see Materials and Methods) not containing a walker and a track, generating *E*-histograms belonging to intact motors only. For sm-FRET/ALEX measurements that indicates the formation of the motor, see S3 in the Supporting Information.

**Low Operational Yield.** Freely diffusing motors at single-molecule concentration (3 pM) were sequentially fed with nonhairpin fuels and the corresponding antifuels (200 nM), and the sample was continuously monitored with the sm-FRET/ALEX technique. After each addition of fuels the sample was incubated for 45 min, and after each addition of antifuel the sample was incubated for 30 min to allow the reaction to complete. Two-dimensional *E*/*S*-histograms measured for the last 15 min of each step are presented in Figure 2A–D. The measured *E* values were predominantly as expected. The minor discrepancies are explained in the Supporting Information (Figure S3) and in the Material and Methods. The increase in the population at $S \sim 0.1$ indicates departure of the walker from the origami track. After six steps (six fuel-addition and six fuel-removal reactions) only about 1% of the motors remained intact (Figure 2D).

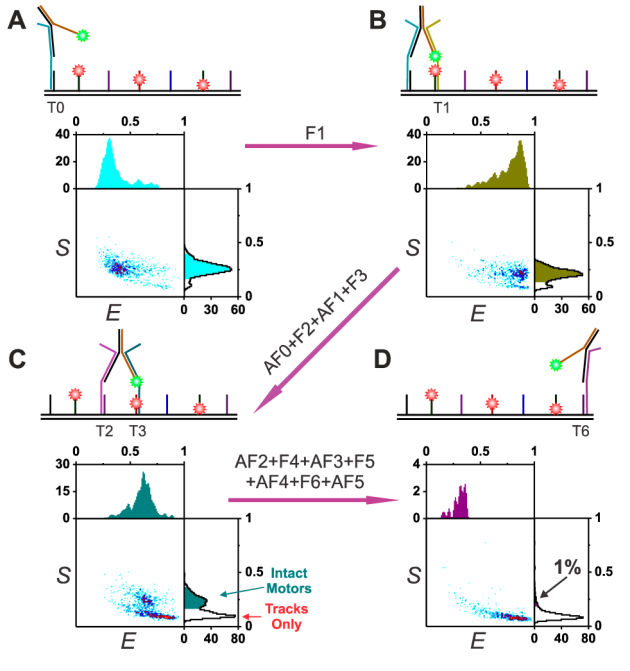


**Figure 2.** Low operational yield. (A–D) Four out of 13 motor states measured with sm-FRET/ALEX. The *E*-histograms report on the motor progress and the *S*-histograms on motor integrity. With each additional step a portion of the walkers detach from the origami track, resulting in an increase of the acceptor-only population (the peaks at *S* ~ 0.1). After the introduction of six fuels and six antifuels, only 1% of the motors remain intact (D).

**The Fuel-Removal Reaction.** To measure the kinetics and yield of the fuel-removal reaction, we introduced different concentrations of antifuel AF1 into a solution of 10 pM freely


dx.doi.org/10.1021/ja4048416 | J. Am. Chem. Soc. 2013, 135, 11935−11941

diffusing motors and continuously monitored the motors using the sm-FRET/ALEX technique (Figure 3). In the initial state

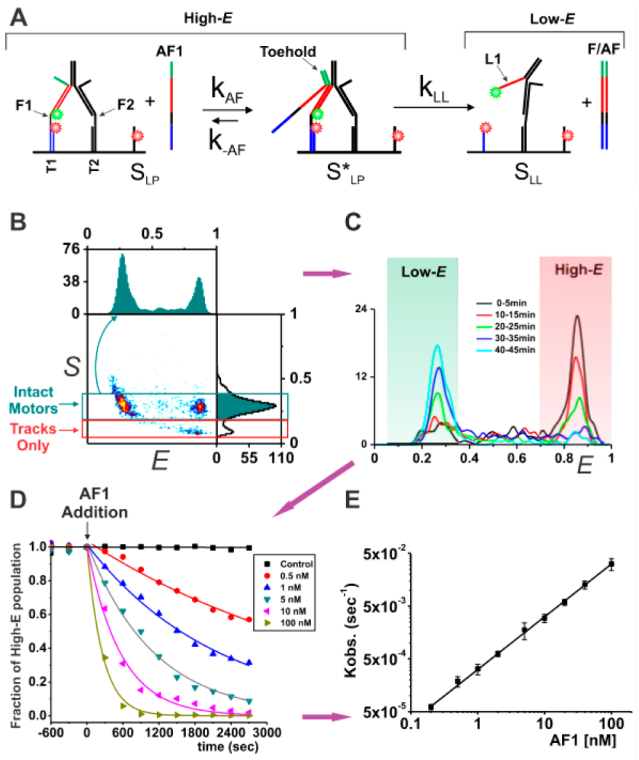


**Figure 3.** Fuel-removal reaction. (A) Mechanism of the fuel-removal reaction. (B) Two-dimensional *E*/*S*-histogram of the motor measured continually from before the introduction of antifuel to 2700 s after. Only populations with the correct stoichiometry were considered for the generation of the kinetic profiles (inside the dark green rectangle). (C) *E*-histograms measured at a different time since the introduction of AF1. (D) Plots of the fractions of high-*E* populations measured at several AF1 concentrations. Each curve is fitted with eq 1, from which $k_{obs}$ is calculated. (E) $k_{obs}$ are plotted as a function of AF1 concentration.

(called leg-placed, $S_{LP}$) the two walker legs are joined by two fuels to two footholds and the *E* values are high ($E = 0.7-1.0$). Upon introduction, the antifuel AF1 binds the fuel toehold, forming state $S^*_{LP}$. This is followed by a toehold-mediated strand displacement, which removes the fuel from the motor, resulting in lifting of L1 and formation of state $S_{LL}$ and a decrease in *E* value. The kinetic profiles of the fuel-removal reactions, defined as the fraction of motors with high *E*, are presented in Figure 3D.

Complete solution of the fuel-removal rate equations are given in the Supporting Information (eqs S1−S12). That the AF1 concentrations are considerably higher than that of the motors justifies a pseudo-first-order assumption for the binding of AF1 to the toehold of F1. The time it takes for a strand to displace another strand in a context of a toehold-mediated strand displacement reaction is around 1 $s^{-1}$.[22] This is significantly faster than our fuel-removal reactions. On the basis of that, we assumed that the rate-limiting step is the binding of AF1 to F1 and not the F1 displacement, justifying a steady-state approximation for $S^*_{LP}$. Therefore, the fraction of high-*E* population should behave according to eq 1:

$$\left(\frac{[\text{high } E]}{[\text{high } E] + [\text{low } E]}\right)_t = \exp(-k_{obs}t) \quad (1)$$

Fitting eq 1 to the data (Figure 3D) shows that $k_{obs}$ is linearly dependent on the AF1 concentration (Figure 3E), validating the rate-limiting-step assumption and the steady-state approximation. From the slope of the graph in Figure 3E (Supporting Information, eqs S11, S12) we calculated the concentration-independent AF1 binding rate constant and found it to be $k_{AF} = (3.14 \pm 0.02) \times 10^5$ $M^{-1}$ $s^{-1}$. This value is in very good agreement with the published rate for hybridization of two strands in a second-order reaction [$(1-5) \times 10^5$ $M^{-1}$ $s^{-1}$],[23−25] further supporting the rate-limiting-step assumption and indicating that the majority of antifuel binding events lead to fuel removal. As indicated by the result (Figure 3D, e.g., the 100 nM AF1 concentration) and explained by the analysis, given enough time and proper antifuel concentrations, the fuel-removal reaction does reach completion. *Therefore, the fuel-removal* reaction *is not the reason for the low operational yield observed.*

**The Fuel-Addition Reaction.** We continued by studying the kinetics and yield of the fuel-addition reaction. The measurements were conducted using the same procedures as for the fuel-removal reaction, except that L1 was already lifted in the initial state (leg-lifted $S_{LL}$, Figure 4A) and fuels, rather

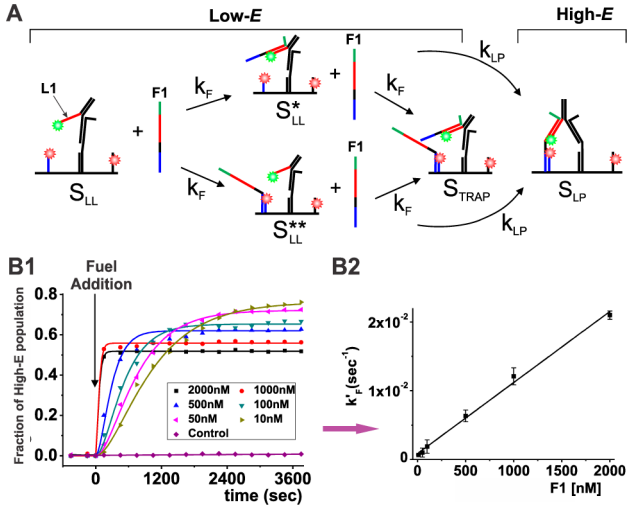


**Figure 4.** Fuel-addition reaction. (A) A proposed mechanism of the fuel-addition reaction using nonhairpin fuel. Instead of one fuel binding the leg or the foothold followed by binding of the other and completion of the reactions, two fuels may bind the motor consecutively, resulting in a trapped state, $S_{TRAP}$. Higher concentrations of fuel increased the probability of forming the trapped state. (B1) Kinetic profiles of the fuel-addition reactions (fraction of high-*E* population) measured at different F1 concentrations and fitted with eq 2. Clearly, an increased concentration of F1 decreases the reaction yield. (B2) Calculated pseudo-first-order rate constants $k'_F$ at different F1 concentrations.

than antifuels, were introduced. The kinetic profiles of the fuel-addition reactions are presented in Figure 4B1. *The most significant observation is that increased fuel concentration decreases, rather than increases, the* reaction *efficiency.*

To explain these important results, we proposed the mechanism presented in Figure 4A. In the intended fuel-addition reaction, a single fuel should binds the foothold (to


dx.doi.org/10.1021/ja4048416 | J. Am. Chem. Soc. 2013, 135, 11935−11941

form state $S_{LL}$). This is followed by an intramolecular reaction in which the same fuel completes the reaction by binding the free leg to form the intended state $S_{LP}$ (alternatively, the fuel may first bind to the foothold and then the leg, state $S_{LL}^{**}$). It is possible, however, that an additional fuel binds to the free leg or foothold in an intermolecular reaction before the first fuel completes the intramolecular reaction, resulting in the formation of a trapped state ($S_{TRAP}$). Because the rate for dissociation of the fuel from the leg and the foothold is very slow (the fuel-foothold and the fuel-leg form duplexes of 17 and 18 base pairs), the motor remains bound to two fuels, and the leg remains lifted. Higher concentrations of fuels increase the rate of formation of intermediates ($S_{LL}^{*}$ and $S_{LL}^{**}$) and increase the rate of formation of the trapped state from the intermediates; however, it does not increase the rate of formation of the desired $S_{LP}$ state from the intermediates. *Thus, according to our models, higher fuel concentrations should reduce the yield of the fuel-addition reaction.*

Complete solution of the fuel-addition rate equations are given in the Supporting Information (eqs S13−S24). We assume a pseudo-first-order reaction for binding a fuel to a leg or to a foothold with a pseudo-first-order fuel-binding rate constant, $k'_F$. For reasons of simplicity, we assume that this rate is equal for fuel binding legs and footholds. We do not expect the origami to cause a significant reduction in the binding rate to the nearby footholds in comparison to the leg[43] under the counterion concentration used (100 mM NaCl).

On the basis of these assumptions, the kinetic profile for the formation of the leg-placed state $S_{LP}$ is given by eq 2.

$$\left(\frac{[\text{high } E]}{[\text{high } E] + [\text{low } E]}\right)_t = \frac{k_{LP}}{k'_F + k_{LP}} + \frac{k_{LP}}{k'_F - k_{LP}} \exp(-2k'_F t) + \frac{2k'_F k_{LP}}{(k'_F + k_{LP})(k'_F - k_{LP})} \exp(-(k'_F + k_{LP})t) \quad (2)$$

Fitting eq 2 to the data (Figure 4B1) shows that $k'_F$ is linearly dependent on the fuel concentration (Figure 4B2), as expected from our model and supporting it. From the slope in this graph (Supporting Information, eq S24) we calculated the concentration-independent fuel-binding rate constant: $k_{AF} = (3.14 \pm 0.02) \times 10^5\ M^{-1}\ s^{-1}$. These rates are 10−30 times slower than expected for binding of two complementary strands to form a duplex, and currently we do not have an explanation for the slow rate. The leg-placing rate, $k_{LP}$, reflects the times it takes to join the leg and the foothold after one of the two is bound to fuel. The values of $k_{LP}$ varied from $(1.67 \pm 0.06) \times 10^{-2}\ s^{-1}$ (~60 s) when 2000 nM fuel was used to $(2.11 \pm 0.05) \times 10^{-3}\ s^{-1}$ (~470 s) when 10 nM fuel was used. According to the model, $k_{LP}$ should not vary with the fuel concentration. Lack of resolution, however, prevented us from determining conclusively whether $k_{LP}$ varies or whether these variations are a result of the influence of a small population of nonreacting motors on the fit.

The reaction yield at infinite time is given in eq 3 (see also Supporting Information, eq S23). *The* equation *shows that higher fuel concentration decreases the yield.*

$$\left(\frac{[\text{high } E]}{[\text{high } E] + [\text{low } E]}\right)_{t=\infty} = \frac{[S_{LP}]_{t=\infty}}{[S_{LL}]_0} = \frac{k_{LP}}{k'_F + k_{LP}} \quad (3)$$

**Rational Design of Hairpin-Fuel.** To reduce limitations on speed and yield caused by the formation of the trapped state, we developed a hairpin-based fuel. Nonhairpin fuels bind the legs and the footholds at roughly the same rate. Our asymmetric hairpin-fuel is designed to bind the foothold first and bind the leg only after binding the foothold (Figure 5A).

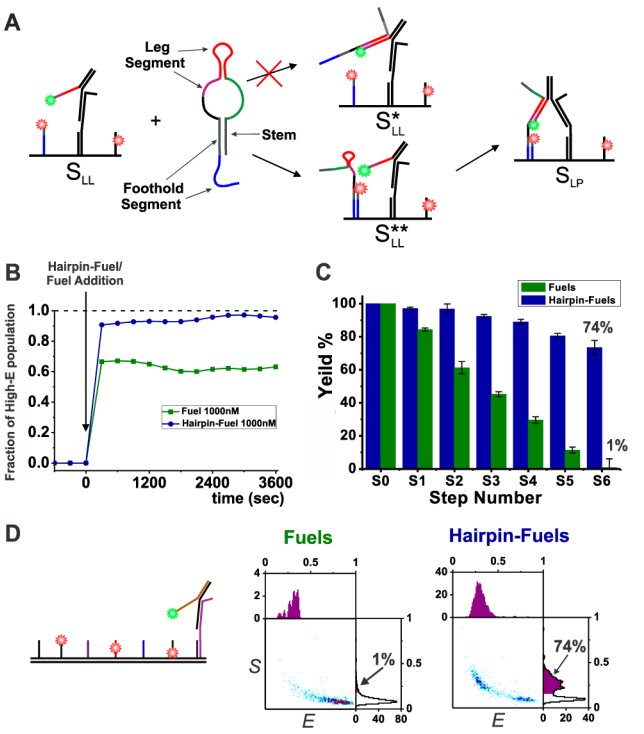


**Figure 5.** Hairpin-fuel. (A) A proposed mechanism of the fuel-addition reaction using hairpin-fuel. (B) A compression of the kinetic profile of the fuel-addition reaction using fuel (green) and hairpin-fuel (blue). (C) A compression of the operational yield of motors operating using fuels and hairpin-fuels measured after each step. (D) A compression of the sm-FRET/ALEX results for motors operating with fuels and hairpin-fuels measured at the sixth step.

This is achieved by placing the segment that is designed to bind the leg (Figure 5A, colored pink and red) inside the hairpin loop and stem, slowing the binding of the fuel to the leg.[44−46] Part of the segment that is designed to bind the foothold is exposed (the blue part) and can bind the foothold at high rate (typical of hybridization of two strands). Upon hybridization of the hairpin-fuel and the foothold, the stem (gray) is opened, exposing the toehold and making it available for binding to the leg to complete the fuel-addition reaction. The kinetic profiles of nonhairpin fuel and hairpin-fuel addition reactions measured at 1000 nM fuel and hairpin-fuel concentrations are compared in Figure 5B. The nonhairpin fuel reaches a maximum of about 65% yield after 150 s (the time resolution of the measurement), whereas the hairpin-fuel reaches 90% after 150 s and 98% after 3000 s. The fraction of motors that did not react properly reduces by 17-fold (from 35% to 2% per reaction). *This significant improvement in the reaction yield demonstrates that the inefficiency observed for the nonhairpin fuel is a result of consecutive binding of fuels, as we proposed, and that our rationally designed hairpin-fuel functions as intended.*

**Successful High-Yield Operation.** After demonstrating that the fuel-addition reaction using hairpin-fuel was significantly more efficient than that with fuel, we measured the


dx.doi.org/10.1021/ja4048416 | J. Am. Chem. Soc. 2013, 135, 11935−11941

motor operational yield using hairpin-fuels. Six hairpin-fuels and six corresponding anti-hairpin-fuels (AHF0−5) were introduced consecutively. Comparisons of the yields measured for motors operated with fuels and with hairpin-fuels and of the sm-FRET/ALEX histograms measured at the sixth step are presented in Figure 5C,D. The results are clear: after six introductions of fuels and six antifuels only 1% of the motors remained intact, whereas after six introductions of hairpin-fuels and six anti-hairpin-fuels as much as 74% of the motors remained intact and operational. *The 2 order-of-magnitude improvement in the overall operational yield, observed after only six consecutive steps, emphasizes the importance of achieving high yields for each individual* reaction.

**Slow and Nonreacting Motors.** The kinetic profiles of the fuel and the hairpin-fuel addition reactions indicate that a small fraction of nonreacting or slowly reacting motors may exists (the nonhairpin fuel and the hairpin-fuel did not reach 100% yield even when introduced in low enough concentrations; data not shown). A possible explanation for this observation is that around 2−8% of the motors populate states in which, because of geometrical considerations, the fuels or hairpin-fuels cannot bridge between the foothold and the leg, and only with time, some of these motors find a way out of these states and complete the reaction (Supporting Information, Figure S3C). Missing footholds may also explain part of the reduced yield (Supporting Information, Figure S3A). These are probably the reason why the operational yield after six steps, using the hairpin-fuel, was only 74%. More single-molecule study is required to explain the reasons for the observed imperfectness and to offer a rational solution.

**Implications for Fast and Reliable Molecular Machines.** Our results suggest that it should be feasible to create fast and efficient DNA-based motors and machines. The data indicate that, given enough time and proper antifuel concentrations, the fuel-removal reaction does reach completion. This indicates that the toehold-mediated strand displacement reaction enables a complete removal of the fuel and that the fuel-removal reaction is not a major cause for the low operational yields observed. In addition, because increased antifuel concentration linearly increased the fuel-removal reaction rate (Figure 3E), it is reasonable to assume that increasing the antifuel concentration beyond the 100 nM tested here will accelerate the fuel-removal reaction further. The strand displacement reaction is expected to slow the fuel-removal reaction only when the antifuel binding rate reaches that of the strand displacement rate, which is around 1 $s^{-1}$.[22] To illustrate, it may be possible to reach 99% fuel removal within 7 s when a 1 $\mu$M antifuel concentration is used.

Furthermore, the results of the fuel-addition reaction show that more than 50% of the motors operated with the fuel and 90% of the motors operated with the hairpin-fuel complete the fuel-addition reaction in less than 150 s (Figure 5B), indicating that intramolecular leg-placing is fast. For the leg-placing reaction to take place, the leg and the foothold must be oriented such that the fuel can bridge between them.[18] This is where the motor actually steps forward, and it is very encouraging that most of the motors overcome this geometrical constraint and execute the striding function, at such promising rates.[18]

Because a high concentration of nonhairpin fuel promotes side reactions (the trapped state in our case), the yield and the rate are compromised. At high fuel concentrations, the reaction is fast but the yield is low, and at low fuel concentrations, the yield is high but the reaction is slow (Figure 4B1), placing limitations on speed, yield, and overall functionality. It is likely that similar unwanted interaction explains the presence of dimers and other complexes observed in previous non-autonomous devices[19,26,27] and by us[38] for an autonomous bipedal motor.[47] *As we demonstrate here, however, this problem can be overcome using asymmetric fuels (or other connecting strands) that regulate the reaction hierarchy.*

## ■ CONCLUSIONS

This study is part of a broader effort to demonstrate truly reliable, stable, and fast DNA-based machines capable of conducting many sequential operations. To this aim, we utilized single-molecule FRET and ALEX techniques and elucidated the mechanisms of the reactions involved in the operation of a DNA-based bipedal motor. The implications for fast and efficient DNA-based molecular machines are mostly positive. Strands can be removed from devices with yields and rates that are high as those of the toehold-mediated strand displacement reaction. Furthermore, trapped states formed when operating machines at high concentration of fuels can be avoided using asymmetrical hairpin-fuels, significantly increasing operational yield. With such rationally designed fuels, machines should be able to operate with better yields, and because higher concentration of fuels can be used, with faster rates. Taken together, these findings bring us closer to molecular machines that operate with yields and speeds approaching that of elementary DNA strands' reactions.

More generally, this study demonstrates how careful and systematic analysis of individual reactions at the single-molecule level can lead to rational optimization of a DNA-based machine and demonstrates that single-molecule fluorescence, based on its ability to provide detailed in situ structural and dynamical information, inaccessible using traditional methods, constitutes an excellent tool for the development of DNA-based nanotechnology.

## ■ MATERIALS AND METHODS

**ssDNA Labeling.** HPLC-purified ssDNAs were purchased (IDT Inc., Coralville, LA) with a C6 dT internal amino modifier (iAmMC6T) in specified positions. ATTO-550 and ATTO-647N (donor and acceptor, respectively, ATTO-TECH GmbH, Siegen, Germany) were labeled and HPLC purified (reverse-phase C18, Amersham Bioscience, Uppsala, Sweden). Typical labeling yields were ∼70% and purities after HPLC were >99% as verified by reintroduction into the HPLC.

**Motor Preparation.** DNA origami was prepared following Rothemund's rectangle.[7] M13mp18 ssDNA was used as scaffold (New England BioLabs), and the staples were ordered unpurified (IDT). The annealing solution was comprised of 2 nM scaffold; 5-fold excess of staples; 20-fold excesses of footholds, fuels, and legs in 40 mM TAE Tris, 1 mM EDTA, and 40 mM acetic acid; and 12.5 mM $MgCl_2$ in a 50 $\mu$L volume. To prevent sticking of the origami to each other, edge staples were not introduced. The annealing procedure was as follows: 95 °C for 5 min, cool to 60 °C at 1 °C/2 min, and cool to 20 °C at 1 °C/5 min. After annealing the origami was washed using a 100-KD filter (Amicon Ultra, Millipore) by centrifuging (5174R, Eppendorf) four times at ∼14 000$g$ for 5 min in 50× TAE and 12.5 mM $MgCl_2$. We found that washing with 50× TAE reduces origami and staple dissociation, resulting in higher recovery of origami from the Amicon and increased presence of footholds as verified by ALEX. Samples were then spun again for 10 min at ∼14 000$g$ in 1× TAE buffer (to remove $Mg^{2+}$ and the 50× TAE) and subjected to a final spin reversed at 1000$g$ for 5 min. For the yield measurements (Figures 2 and 5C,D) all seven footholds were introduced in the annealing


dx.doi.org/10.1021/ja4048416 | J. Am. Chem. Soc. 2013, 135, 11935−11941

process, and for the kinetic measurements (Figures 3–5) only footholds T0, T1, and T2 were introduced. The footholds are designed to branch out of the origami in the locations of staples r-7t10f, r-7t10e, r-5t10f, r-5t10e, r-3t10f, and r-3t10 (see ref 7). To avoid competition, these staples were not introduced. For the yield measurements F0 and F1 or HF0 and HF1 were introduced in the annealing process such that the walker parked at the beginning of the track. For the fuel-removal measurements (Figure 3), F1 and F2 were introduced such that the walker parked on T1 and T2. For the fuel-addition measurement (Figure 4), AF1 was introduced before the final spin/wash to lift L1 from T1.

**Measurement of the Motor Operational Yield.** Motor progress (Figures 2 and 5C,D) was monitored in one continuous measurement. A sample (50 $\mu$L of 3 pM motor) was placed on a coverslip and sealed with silicone. The low concentration reduces the probability of observing more than one device at a time. An upper coverslip was gently placed on the silicon and removed briefly for introduction of fuels or antifuels. The bottom coverslip was KOH-treated by sonication (15 min) in 1 M KOH solution, thoroughly washed with distilled water, and dried with air. This treatment makes the coverslip negatively charged, preventing sticking of the negatively charged origami as confirmed by TIRF measurements. The measurement buffer was comprised of 10 mM Tris (pH 8), 1 mM EDTA, 10 $\mu$g/mL BSA (Sigma-Aldrich) to reduce sample sticking, 500 mM NaCl, and 1 mM Trolox (Sigma-Aldrich) to reduce fluorophore photobleaching and photoblinking. Fuels and antifuels were introduced sequentially (200 nM final concentration). Data were collected during the entire operation period, but data from only the last 15 min, after most of the motors reacted, are presented. Binding of donor labeled L1 to acceptor labeled T1, T3, and T5 yielded $E$ values of approximately 0.85, 0.6, and 0.5, respectively, and the $E$ value of a lifted L1 was 0.3. This is in a good agreement with $E$ values estimate from measurement of dsDNA (data not shown). Although there were some overlaps between the $E$-histograms of the different states, there was no overlap with the leg-lifted histograms, enabling complete separation of the initial and the final states in all measurements. On the basis of the definition of $S$ (eq 5), acceptor only events ($S < 0.13$) were considered as origami tracks that have lost the walker, and events having three acceptors and one donor ($0.37 > S > 0.13$) were considered intact motors. These exact values were chosen to achieve best separation between the somewhat overlapped populations.

**Measurement of the Kinetic Profiles.** Motors were placed on a coverslip and sealed with silicone and an upper coverslip. To increase the statistics, and therefore the time resolution, 10 pM motor was used for the kinetic measurements. The measurement buffer consisted of 10 mM Tris (pH 8), 1 mM EDTA, 10 $\mu$g/mL BSA, 1 mM Trolox, and 100 mM NaCl. The reaction profiles in Figure 4B1 were measured in 1000 mM NaCl. Fuel and antifuel were added after 450 s (considered as time equal zero) from a 10× stock solution (relative to the final concentration), achieving final volume of 50 $\mu$L. Data were collected for around 120 min. The data was divided into chunks of 300 s, and the ratio of high-$E$ divided by the sum of high-$E$ and low-$E$ (high-$E$ defined as $E$ = 0.7–1 and low-$E$ defined as $E$ = 0.05–0.35) was calculated.

**Data Analysis and Presentation.** Data analysis was performed with the in-house-written Labview (National Instruments v 7.1) software as described previously.[38,42] The beginnings and ends of bursts were determined by the all-photons-burst-search (APBS, parameters: $L$ = 2000, $M$ = 100, and $T$ = 2500 $\mu$s). For each burst, $E$ and $S$ were calculated according to eqs 4 and 5, respectively, binned (0.01 $E$ bin size), and plotted on one-dimensional $E$ and $S$ histograms and on a two-dimensional $E/S$ histogram.

**Calculation of *E* and *S*.** In ALEX experiments,[38−42] two lasers alternatively excite the donor and the acceptor dyes; therefore, the calculation of $E$ is somewhat different from that in a conventional single laser experiment and is based on eq 4

$$E = \frac{A_{D_{EX}}}{D_{D_{EX}} + A_{D_{EX}}} \quad (4)$$

where $D_{D_{EX}}$ is the number of photons recorded in the donor channel and $A_{D_{EX}}$ is the number of photons recorded in the acceptor channel during times in which the donor laser is on (donor laser "on time"), as commonly defined in ALEX experiments.[38] Stoichiometry, $S$, is calculated by dividing the sum of the photons recorded in the donor and the acceptor channels during donor laser on time by the sum of the photons recorded in both channels during donor laser and acceptor laser on times (eq 5)

$$S = \frac{D_{EX}}{D_{EX} + A_{EX}} \quad (5)$$

where $D_{EX}$ and $A_{EX}$ are the sums of photons recorded in the donor and the acceptor channels during donor laser and acceptor laser on times, respectively.

**Optical Setup.** The sm-FRET/ALEX experiments were carried out on an in-house-built optical setup. A detailed description can be found in the Supporting Information and in previous publications.[38,41,42]

## ■ ASSOCIATED CONTENT

### Ⓢ Supporting Information

Sequences of the DNA strands, solution of the rate equations, principles of the sm-FRET/ALEX technique, optical setup, and additional data. This material is available free of charge via the Internet at http://pubs.acs.org.

## ■ AUTHOR INFORMATION

### Corresponding Author

Eyalnir@bgu.ac.il

### Notes

The authors declare no competing financial interest.

## ■ ACKNOWLEDGMENTS

E.N. was supported by the Alon Fellowship, T.T. was supported by the Negev Fellowship, and M.L was supported by the Darom Fellowship.

## ■ REFERENCES

(1) Toprak, E.; Yildiz, A.; Hoffman, M. T.; Rosenfeld, S. S.; Selvin, P. R. *Proc. Natl. Acad. Sci. U. S. A.* **2009**, *106*, 12717.
(2) Seeman, N. C. *Trends Biochem. Sci.* **2005**, *30*, 119.
(3) Bath, J.; Turberfield, A. J. *Nat. Nanotechnol.* **2007**, *2*, 275.
(4) Pinheiro, A. V.; Han, D. R.; Shih, W. M.; Yan, H. *Nat. Nanotechnol.* **2011**, *6*, 763.
(5) Beissenhirtz, M. K.; Willner, I. *Org. Biomol. Chem.* **2006**, *4*, 3392.
(6) Simmel, F. C. *Curr. Opin. Chem. Biol.* **2012**, *23*, 1.
(7) Rothemund, P. W. K. *Nature* **2006**, *440*, 297.
(8) Wei, B.; Dai, M. J.; Yin, P. *Nature* **2012**, *485*, 623.
(9) Jungmann, R.; Scheible, M.; Kuzyk, A.; Pardatscher, G.; Castro, C. E.; Simmel, F. C. *Nanotechnology* **2011**, *22*, 275301.
(10) Douglas, S. M.; Dietz, H.; Liedl, T.; Hogberg, B.; Graf, F.; Shih, W. M. *Nature* **2009**, *459*, 414.
(11) Dietz, H.; Douglas, S. M.; Shih, W. M. *Science* **2009**, *325*, 725.
(12) Han, D. R.; Pal, S.; Nangreave, J.; Deng, Z. T.; Liu, Y.; Yan, H. *Science* **2011**, *332*, 342.
(13) Bai, X. C.; Martin, T. G.; Scheres, S. H. W.; Dietz, H. *Proc. Natl. Acad. Sci. U. S. A.* **2012**, *109*, 20012.
(14) Douglas, S. M.; Marblestone, A. H.; Teerapittayanon, S.; Vazquez, A.; Church, G. M.; Shih, W. M. *Nucleic Acids Res.* **2009**, *37*, 5001.
(15) Kim, D. N.; Kilchherr, F.; Dietz, H.; Bathe, M. *Nucleic Acids Res.* **2012**, *40*, 2862.
(16) Castro, C. E.; Kilchherr, F.; Kim, D. N.; Shiao, E. L.; Wauer, T.; Wortmann, P.; Bathe, M.; Dietz, H. *Nat. Methods* **2011**, *8*, 221.
(17) Arbona, J. M.; Aime, J. P.; Elezgaray, J. *Phys. Rev. E* **2012**, *86*, 051912.

(18) Ouldridge, T. E.; Hoare, R. L.; Louis, A. A.; Doye, J. P. K.; Bath, J.; Turberfield, A. J. *ACS Nano* **2013**, *7*, 2479.
(19) Yurke, B.; Turberfield, A. J.; Mills, A. P.; Simmel, F. C.; Neumann, J. L. *Nature* **2000**, *406*, 605.
(20) Li, Q. Q.; Luan, G. Y.; Guo, Q. P.; Liang, J. X. *Nucleic Acids Res.* **2002**, *30*, e5.
(21) Zhang, D. Y.; Seelig, G. *Nat. Chem.* **2011**, *3*, 103.
(22) Zhang, D. Y.; Winfree, E. *J. Am. Chem. Soc.* **2009**, *131*, 17303.
(23) Henry, M. R.; Stevens, P. W.; Sun, J.; Kelso, D. M. *Anal. Biochem.* **1999**, *276*, 204.
(24) Lehr, H. P.; Reimann, M.; Brandenburg, A.; Sulz, G.; Klapproth, H. *Anal. Chem.* **2003**, *75*, 2414.
(25) Michel, W.; Mai, T.; Naiser, T.; Ott, A. *Biophys. J.* **2007**, *92*, 999.
(26) Simmel, F. C.; Yurke, B. *Phys. Rev. E* **2001**, *63*, 041913.
(27) Muller, B. K.; Reuter, A.; Simmel, F. C.; Lamb, D. C. *Nano Lett.* **2006**, *6*, 2814.
(28) Feng, L. P.; Park, S. H.; Reif, J. H.; Yan, H. *Angew. Chem. Int. Ed.* **2003**, *42*, 4342.
(29) Chakraborty, B.; Sha, R.; Seeman, N. C. *Proc. Natl. Acad. Sci. U. S. A.* **2008**, *105*, 17245.
(30) Goodman, R. P.; Heilemann, M.; Doose, S.; Erben, C. M.; Kapanidis, A. N.; Turberfield, A. J. *Nat. Nanotechnol.* **2008**, *3*, 93.
(31) Andersen, E. S.; Dong, M.; Nielsen, M. M.; Jahn, K.; Subramani, R.; Mamdouh, W.; Golas, M. M.; Sander, B.; Stark, H.; Oliveira, C. L. P.; Pedersen, J. S.; Birkedal, V.; Besenbacher, F.; Gothelf, K. V.; Kjems, J. *Nature* **2009**, *459*, 73.
(32) Zadegan, R. M.; Jepsen, M. D. E.; Thomsen, K. E.; Okholm, A. H.; Schaffert, D. H.; Andersen, E. S.; Birkedal, V.; Kjems, J. *ACS Nano* **2012**, *6*, 10050.
(33) Graugnard, E.; Kellis, D. L.; Bui, H.; Barnes, S.; Kuang, W.; Lee, J.; Hughes, W. L.; Knowlton, W. B.; Yurke, B. *Nano Lett.* **2012**, *12*, 2117.
(34) Sherman, W. B.; Seeman, N. C. *Nano Lett.* **2004**, *4*, 1203.
(35) Shin, J. S.; Pierce, N. A. *J. Am. Chem. Soc.* **2004**, *126*, 10834.
(36) Tian, Y.; Mao, C. D. *J. Am. Chem. Soc.* **2004**, *126*, 11410.
(37) Gu, H. Z.; Chao, J.; Xiao, S. J.; Seeman, N. C. *Nature* **2010**, *465*, 202.
(38) Masoud, R.; Tsukanov, R.; Tomov, T. E.; Plavner, N.; Liber, M.; Nir, E. *ACS Nano* **2012**, *6*, 6272.
(39) Kapanidis, A. N.; Laurence, T. A.; Lee, N. K.; Margeat, E.; Kong, X.; Weiss, S. *Acc. Chem. Res.* **2005**, *38*, 523.
(40) Kapanidis, A. N.; Lee, N. K.; Laurence, T. A.; Doose, S.; Margeat, E.; Weiss, S. *Proc. Natl. Acad. Sci. U. S. A.* **2004**, *101*, 8936.
(41) Nir, E.; Michalet, X.; Hamadani, K. M.; Laurence, T. A.; Neuhauser, D.; Kovchegov, Y.; Weiss, S. *J. Phys. Chem. B* **2006**, *110*, 22103.
(42) Tomov, T. E.; Tsukanov, R.; Masoud, R.; Liber, M.; Plavner, N.; Nir, E. *Biophys. J.* **2012**, *102*, 1163.
(43) Jungmann, R.; Steinhauer, C.; Scheible, M.; Kuzyk, A.; Tinnefeld, P.; Simmel, F. C. *Nano Lett.* **2010**, *10*, 4756.
(44) Green, S. J.; Lubrich, D.; Turberfield, A. J. *Biophys. J.* **2006**, *91*, 2966.
(45) Turberfield, A. J.; Mitchell, J. C.; Yurke, B.; Mills, A. P., Jr.; Blakey, M. I.; Simmel, F. C. *Phys. Rev. Lett.* **2003**, *90*, 118102.
(46) Chen, C. L.; Wang, W. J.; Wang, Z.; Wei, F.; Zhao, X. S. *Nucleic Acids Res.* **2007**, *35*, 2875.
(47) Omabegho, T.; Sha, R.; Seeman, N. C. *Science* **2009**, *324*, 67.